· Review ·
doi: 10.13679/j.advps.2016.2.00090

Advances in Polar Science
June 2016 Vol. 27 No. 2: 90-101

Climate and meteorological processes of the East Antarctic ice sheet between Zhongshan and Dome-A

BIAN Lingen[1*], Ian Allison[2], XIAO Cunde[3], MA Yongfeng[1], FU Liang[1] & DING Minghu[1]

[1] Chinese Academy of Meteorological Sciences, Beijing 100081;
[2] Antarctic Climate and Ecosystems CRC, Private Bag 80, Hobart, TAS 7001, Australia;
[3] State Key Laboratory of Cryospheric Science, Cold and Arid Regions Environmental and Engineering Research Institute, Chinese Academy of Sciences, Lanzhou, China

Received 23 April 2016; accepted 23 June 2016

Abstract The 1228 km over-snow traverse route between the Chinese Zhongshan Station, on the coast of Prydz Bay, and Dome-A, at 4091 m elevation the highest point of the East Antarctic ice sheet, has been the focus of CHINARE surface meteorological and climate studies since 2002. A network of seven Automatic Weather Stations has been deployed along this section, including at Dome-A itself, and some of these have now provided nearly-hourly data for over a decade. Atmospheric boundary layer turbulence and radiation observations have been made over the near-coastal ice sheet inland of Zhongshan and surface turbulence measurements using an ultrasonic anemometer system have also been made in the deep interior of the ice sheet. Summer GPS radiosonde soundings of the atmospheric boundary layer have been made at Kunlun Station, near Dome-A. In this paper these observations are combined to provide a comprehensive overview of the meteorological regime of this region of the ice sheet, its climate variability, and as a reference for future study of climate change. This includes investigation of the variation of surface climate features with elevation and distance from the coast, the height and structure of the boundary layer over the ice sheet, and seasonal and regional changes in ice/snow–air interactions, including turbulent and radiative energy fluxes. The air temperature and snow temperature between the coastal Zhongshan and Dome-A on the inland plateau have not changed significantly in the past decade compared with the inter-annual variability.

Keywords **Antarctic meteorology, boundary layer, Dome-A climate, automatic weather stations**

Citation: Bian L G, Allison I, Xiao C D, et al. Climate and meteorological processes of the East Antarctic ice sheet between Zhongshan and Dome-A. Adv Polar Sci, 2016, 27: 90-101, doi:10.13679/j.advps.2016.2.00090

1 Introduction

A total of 98% of the Antarctic continent is covered by ice and snow and the continent is a major heat sink in the global climate system. Antarctic processes also play an important role in the global balance of the physical quantities of heat, momentum, and water vapor and therefore directly affect changes in global atmospheric circulation, ocean circulation, weather, and climate[1]. Automatic weather stations (AWS) allow long-term observations of surface meteorological processes and of climate in the Antarctic inland. For example, Schwerdtfeger[2] analyzed Antarctic climate features using early AWS data, and Allison and Morrissy[3] described the first-generation of Australian Antarctic AWS. AWS have been used to investigate the surface climate features of the East Antarctic ice sheet between 100°E and 140°E[4] and of the interior of the Lambert Glacier Basin[5]. Such studies showed that, although AWS operating in the hostile Antarctic environment had some deficiencies, the data could be used to comprehensively study the weather and climate of the Antarctic.

Knowledge of the energy exchange process between ice or snow of the Antarctic and the atmosphere is critical to correctly assess the influence of the Antarctic region on global climatic change, and AWS have also been used to investigate

* Corresponding author, E-mail: blg@camscma.cn

the heat flux, and seasonal cycle of the energy balance over Antarctic snow and ice surfaces in a number of studies[6-14]. For example, van den Broeke et al.[15] studied the seasonal cycle of the Antarctic surface energy balance and variations in components of the energy balance between different regions (coastal region, katabatic wind region, and inland plateau) using four-years of data from AWS in Dronning Maud Land.

Turner et al.[16] analyzed changes in Antarctic climate, including long-term trends of surface air temperature, air pressure, and wind speed, using data from both habited stations and AWS. However, many uncertainties remain in the results because of the patchy geographic coverage of observations and the short duration of some records.

Investigating features of turbulent flow over the ice sheet in different Antarctic regions is also necessary for determining an appropriate boundary layer parameterization for use in numerical weather and climate models. Antarctic turbulence observations are mostly available for short periods in summer, whereas whole-year observations are more scarce in the cold interior because of difficulties in maintaining instruments. Since the establishment of Great Wall Station (62°12'S, 58°57'W) in 1984 and Zhongshan Station (ZS) (69°22'S, 76°22'E) in 1989, the Chinese National Antarctic Research Expedition (CHINARE) has measured radiation and surface micro-meteorological profiles and made turbulence observations near the two coastal stations. These have provided understanding of thermal and dynamic processes in the boundary layers of the Antarctic coastal regions[17-20]. However, research into features of turbulent flow in the boundary layer in the Antarctic inland plateau over a full year is limited.

Since the 18th CHINARE in 2005, AWS have been installed along the 1228 km traverse route between ZS and Dome-A[21], the highest point of the Antarctic Ice Sheet (80°22'S, 77 21'E, 4091 m asl) in collaboration with both the Australian Antarctic Division and the University of Wisconsin in order to obtain a long series of surface meteorological observations[22-23]. During the 27th and 28th CHINAREs, a GPS radiosonde experiment was conducted that measured the vertical structure of the summer atmosphere at Kunlun Station (80°25'S, 77 07'E) near Dome-A[24-26]. The 27th CHINARE also established Taishan summer station (76°58'S, 73°51'E), installed a Chinese-constructed AWS there, and conducted surface turbulent observations using an ultrasonic anemometer system. Observations of short-term climate features, turbulent fluxes, and interaction between snow/ice and the atmosphere in the Antarctic inland have also been made between ZS and Dome-A. These have contributed to evaluation of the representation of atmospheric boundary layer-surface processes in a regional climate model[27] and the variations with topography of near-surface wind and temperature structures[28]. After first correcting for changes in AWS sensor height with snow accumulation[22], Xie et al.[29-31] used the ZS –Dome-A AWS data to assess surface temperature and air pressure data in five reanalysis data sets. These works are crucial for the research into climate variability and change in the region.

In this present work, meteorological observations for the section between ZS and Dome-A, which are now available for more than a decade, and the analyses of these are presented to summarize the meteorological regime of the region and as a reference for future study of climate change.

2 Meteorological observations between ZS and Dome-A

There are relatively few data on the climate of the Antarctic interior or on interaction between ice/snow and the atmosphere there. The development and use of AWS has enabled long-term observations to be automatically made in these hostile weather environments. In the past three decades, approximately one hundred AWS have been deployed in Antarctica, in regions including the Ross Ice Shelf [32], the Lambert Glacier Basin[5], Mizuho Plateau[33], and Dronning Maud Land[34], thereby establishing a comprehensive foundation for studies of ice/snow–air interactions in many Antarctic inland regions. Since the 1980s, Chinese research in Antarctic atmospheric science has expanded significantly. In the 21st century, this has focused on the area between ZS, in the Larsemann Hills on the coast of Prydz Bay, and Dome-A. Since 2002, CHINARE has collaborated with the Australian Antarctic Division to deploy and operate four AWS (LGB69, Eagle, Dome-A, and Panda-N) on the region of the ice sheet between ZS and Dome-A. An additional AWS (Panda-S), was deployed in the Dome-A region in 2008 in collaboration with the University of Wisconsin. In 2011 and 2013, two Chinese-constructed AWS were deployed at Panda-1 and at Taishan mid-way between ZS and Dome-A. These two AWS include long-wave and short-wave radiometers and have obtained obtain whole-of-year wind speed and direction observation data. The AWS locations and settings are shown in Figure 1 and Table 1; details of the instruments used on the AWS and at Zhongshan are given in Tables 2 and 3[21-23, 39-40].

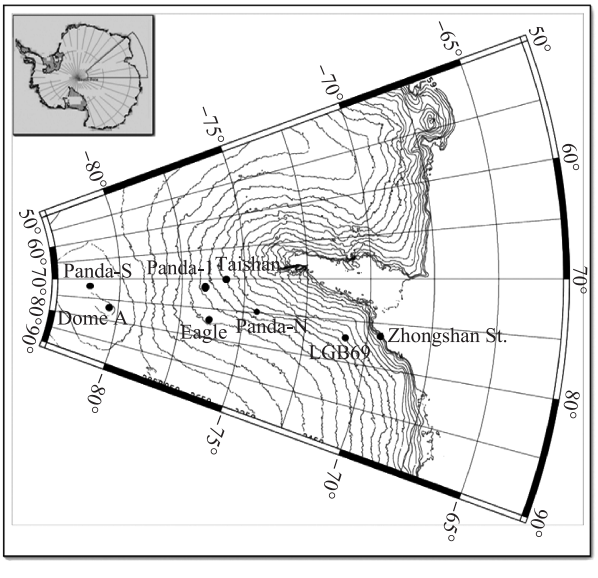

Figure 1 Location of AWS between ZS and Dome-A

Table 1 AWS locations and environmental parameters

AWS name	Lat./S	Long./E	Elevation /(m asl)	Distance to coast/km	Ice sheet surface slope/ ($m \cdot km^{-1}$)	Data availability
Zhongshan	69°22′	76°22′	15	20	0	1989.2 – 2016
LGB69	70°50′	77°04′	1854	180	12.3	2002.1 – 2008.8
Panda-N	73º41’	76º58’	2584	800	3.3	2008.1 – 2016
Taishan	76º58′	73º51′	2626	520	3.7	2013.1 – 2016
Panda-1	77º00′	74º39′	2737	580	3.5	2011.12 – 2013.1
Eagle	76º25’	77º01’	2852	787	3.4	2005.1 – 2016
Panda-S	81º19’	75º59’	4027	1360	0	2008.1 – 2016
Dome-A	80º22’	77º22’	4091	1248	0	2005.1 – 2016

Table 2 Instrument specifications for AWS at LGB69, Panda-N, Eagle and Dome-A

Sensor	Type	Range	Resolution
Air temperature	FS23D thermistor	−85°C– 65°C	0.02°C
Relative humidity	Vaisala HMP45D	0 – 100%	2% (RH<90%) 3% (RH>90%)
Wind speed	Young P/L cup anemometer	0 – 51 $m \cdot s^{-1}$	0.1 $m \cdot s^{-1}$
Wind direction	Aanderra 3590 vane	0° – 360°	6°
Snow height	Campbell Scientific SR50-45	0.5 – 10 m	0.01 m
Global radiation	Middleton EP08	0 – 205 $MJ \cdot m^{-2}$	0.1 $MJ \cdot m^{-2}$
Air pressure	Paroscientific Digiquartz 6501A	500 – 1100 hPa	0.1 hPa
Subsurface temperature	FS23D thermistor	−85°C to 65°C	0.02°C

Table 3 Instrument specifications for Zhongshan weather station and AWS at Taishan, Panda-1 and Panda-S

Sensor	Type	Range	Resolution
Air temperature	Vaisala HMP155	−80°C– 40°C	±0.01°C
Relative humidity	Vaisala HMP155	0 – 00%	2% (RH<90%) 3% (RH>90%)
Wind speed	Propeller type XFY3-1	0 – 95 $m \cdot s^{-1}$	0.2 $m \cdot s^{-1}$
Wind direction	Propeller type XFY3-1	0° – 360°	6°
Radiation	Kipp & Zonen CNR1	0 – 2000 $W \cdot m^{-2}$	0.5 $W \cdot m^{-2}$
Air pressure	Vaisala CS106	600 – 1100 hPa	0.1 hPa

In the summer of 2008, the 24th CHINARE conducted atmospheric boundary layer turbulence observations on the ice sheet about 6 km southeast of ZS. In January 2009, CHINARE established the summer Kunlun Station in the Dome-A region. This station is located 7.3 km southeast of the summit of Dome-A at an elevation of 4087 m. Long-term comprehensive observations in many disciplines, including astronomy, geology, meteorology, and space physics, have been carried out here. Summer GPS radiosonde soundings were made at Kunlun Station from January 7 to 16, 2012 (23 soundings) and from January 8 to 18, 2013 (17 soundings). Profiles of atmospheric pressure, temperature, humidity, wind direction, and wind speed were measured. The maximum height reached by the radiosondes was 15.6 km, with a height of 12 km exceeded 20 times, and the lowest temperature recorded was −73°C. Analyses were made of short-term climate features such as katabatic wind, drift snow flux, ice–air interactions, and boundary layer structure between ZS and Dome-A. The AWS and other data were also used to validate regional climate model simulations and weather model reanalysis data.

3 The near surface climate between ZS and Dome-A

3.1 Basic climate parameters and their change along the section

Based on topographic and climatic features, the ZS to Dome-A section may be divided into four parts. These are the coastal area, the steep escarpment (strong katabatic wind area), plateau with small slope, and the inland plateau.

Many previous studies have been made of the weather and climate in the coastal and steep escarpment regions[35–38]. From analysis of the meteorological data between 1989 and 2008, Bian et al.[39-40] determined that the ZS coastal area has low temperature (coldest recorded, −45.7°C), strong winds (highest gust speed of 50.3 $m \cdot s^{-1}$), and frequent snowstorms (precipitation on 142 $d \cdot a^{-1}$).

Ma et al.[23] analyzed the near surface climate of the traverse route from ZS to Dome-A for the period 2005 to 2007, showing that air temperature, snow temperature, snow accumulation rate, specific humidity, and other meteorological conditions decreased with increasing elevation and distance from the coast. The annual average temperature for this period decreased from −9.2°C at ZS to −51.2°C at Dome-A, with −82.5°C being the lowest temperature recorded during this period at Dome-A. Average specific humidity declined rapidly from 1.154 $g \cdot kg^{-1}$ in the coastal region to 0.044 $g \cdot kg^{-1}$ at Dome-A on the inland plateau, and the accumulation rate decreased from 0.199 m(w.e.)$\cdot a^{-1}$ at LGB69 to 0.032 m (w.e.)$\cdot a^{-1}$ at Dome-A. Wind speed first increased from the coastal to the steep escarpment region and then rapidly decreased toward the inland plateau. The maximum wind speed occurred at LGB69, where the surface slope was greatest, whereas the minimum wind speed was observed at Dome-A with an annual average wind speed of 2.1 $m \cdot s^{-1}$. The constancy of the wind direction (defined as the ratio of the magnitude of the mean wind vector to the scalar average wind speed) was high in the region with strong katabatic wind, whereas wind direction in the coastal region and on the inland plateau showed low constancy.

Variation in the annual averages of basic surface meteorological parameters along the ZS to Dome-A route are shown in Table 4 over the full periods at each station when complete annual data are available. The monthly and annual averages for each individual year for these (and many other Antarctic AWS) are freely available at http://aws.acecrc.org.au/. The full (almost hourly) data from these AWS can be downloaded from the same website in netcdf format.

Figure 2 shows the seasonal variability of the surface lapse rate (γ) between LGB69 (1854 m asl) and Eagle (2852 m) and between Eagle and Dome-A (4091 m) in 2005. On the lower parts of the ice sheet between LGB69 and Eagle the temperature decrease with elevation is super-adiabatic at 1.2°C·(100 m)$^{-1}$. On the inland plateau with lower surface slope the temperature decreases on average at 0.8°C·(100 m)$^{-1}$ of elevation.

Another parameter measured at the ice sheet sites is the height of a fixed point on the AWS above the snow surface (SSH). This decreases with time as new snow accumulates beneath the AWS and, provided the density of the surface snow is known, provides a measure of the accumulation rate and variability. The time series of SSH at Eagle and Dome-A, from 2005 to 2014, is shown in Figure 3. At Dome-A, the surface height decreased at an average rate of 0.15 $m \cdot a^{-1}$ which, for a measured snow density of 250 $kg \cdot m^{-3}$, is equivalent to an accumulation rate of 0.037 m

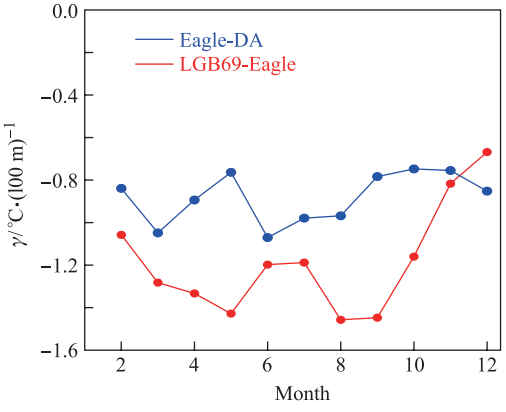

Figure 2 Monthly values of the surface lapse rate between LGB69 and Dome-A in 2005.

Table 4 Annual means of key surface meteorological variables at sites between Zhongshan and Dome-A (see Figure 1). These are multi-year averages over the periods indicated; standard deviations (stdev) are between individual annual averages in the record

Station	Elevn. /m	Years averaged	2 m air temp. /°C		(4 m—1 m) temp. diff /°C		10 m firn temp. /°C		Relative humidity /%		Pressure /hPa		Wind speed[1, 2] /(m·s^{-1})	
			av	stdev	av	stdev	Av	stdev	av	stdev	av	stdev	av	stdev
Zhongshan	15	1989-2014	-9.9	0.8	n/a	n/a	n/a	n/a	58	6.9	984.9	1.9	7.0	0.4
LGB69	1854	2002-2006	-26.2	0.8	0.9	0.4	-27.1	0.04	71	0.9	774.1	1.1	9.2	0.4
Panda-N[3]	2584	2013-2014	-34.2	0.4	0.2	0.1	-35.3	0.08	58	0.5	702.0	0.9	7.9	
Eagle	2830	2005-2014	-41.6	1.0	0.8	0.5	-43.1	0.07	53	1.5	683.0	1.9	4.0	0.4
Dome-A	4091	2005-2014	-52.1	0.8	3.4	0.5	-58.1	0.04	42	1.2	572.6	1.8	2.7	0.2

Notes: [1] Wind speed is measured at 10 m height at ZS, 2 m at Dome-A, and 4 m at other AWS sites.

[2] Wind speed averages at the AWS sites are only over the warmer months when anemometers functioned properly, not annual averages. At LGB 69 this was Sep.−May; at Panda-N, Dec.−Feb.; at Eagle, Nov.−Feb.; and at Dome-A, Nov.−Mar.

[3] Only 2 full years of data are available for Panda-N, and only one of these (2013) has wind speed data.

(w.e.)·a^{-1}, similar to the value of 0.032 m(w.e.)·a^{-1} obtained by Ma et al.[20]. At Eagle the average height decrease was 0.27 m·a^{-1}, equivalent to an accumulation rate of 0.081 m(w.e.)·a^{-1} for a measured snow density of 300 kg·m^{-3}.

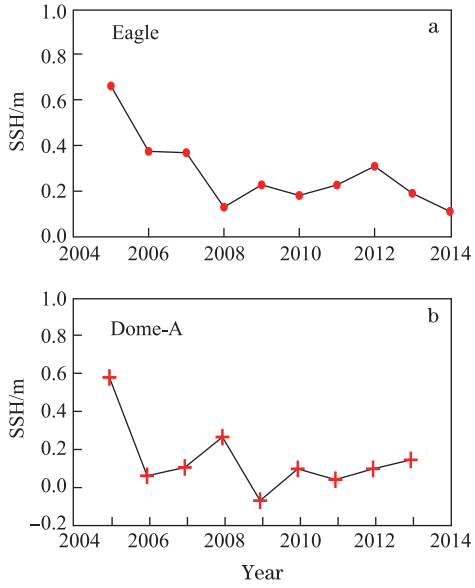

Figure 3 Annual snow surface height (SSH) change from 2005 to 2014 at Eagle (**a**) and Dome-A (**b**).

Note that the snow surface height change in the first year (2005) at both stations is high. This may be an artefact caused by surface disturbance when the stations were deployed.

Ding et al.[41] evaluated the mass balance of the Dome-A region by surface mass balance (SMB) measurements from 2008 to 2013 using 49 stakes installed across a 30 km by 30 km area. The snow surface elevation has increased at a rate of 1.37 kg·m^{-2} annually because the snow accumulation is greater than ice flow discharge at this site; that is, the site is positively out of mass balance. Although the precision of these data requires further confirmation, such observations can provide validation for large-scale Antarctic Ice Sheet changes derived from satellite data.

Xiao et al.[42-43] studied ice sheet and climate features of the Dome-A region using shallow ice core and AWS data. They determined that Dome-A may be an area with suitable conditions, including a very low snow accumulation rate, for recovering a deep ice core more than a million years old.

3.2 Surface climate variability and recent change

Between 1989 and 2014, the temperature at ZS increased at a rate of only 0.04°C·(10 a)$^{-1}$ (Figure 4) while at the nearby Davis Station it has risen at 0.07°C·(10 a)$^{-1}$, indicating little short-term temperature change over the coastal area of Prydz Bay. Figure 4 shows that over this period the annual minimum temperature and annual maximum wind speed at ZS have both tended to decrease[39]. From 2005 to 2014, the annual mean temperature at ZS and Davis Station, both

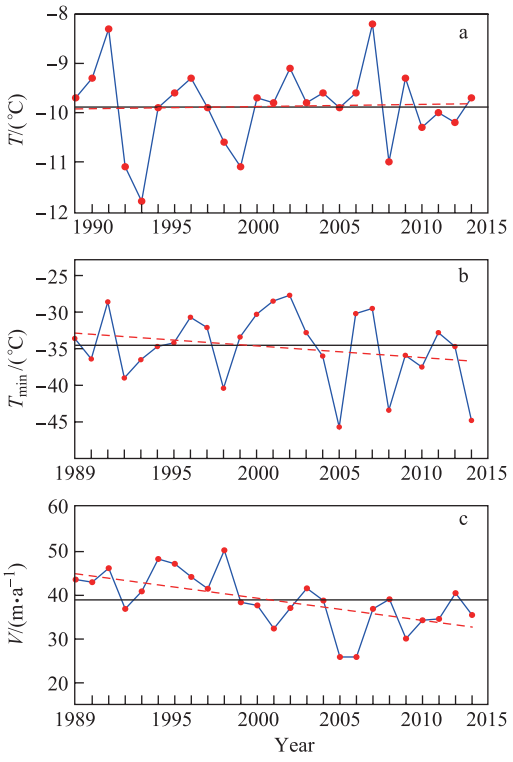

Figure 4 Annual mean temperature (**a**), annual minimum temperature (**b**) and annual maximum wind speed (**c**) at ZS from 1989 to 2014.

in the coastal region, exhibited similar variability and an insignificant decreasing trend within much larger interannual variability of about 3°C (Figure 5).

The meteorological data from the ZS to Dome-A AWS network are now continuously available for more than a decade since 2005, enabling more detailed studies of climate features over the section. Although this period is not long enough to assess climate change, it does provide an indication of climate variability (Figure 5).

Temperature was also measured at four depths to 10 m in the firn at some of the inland AWS sites. The annual mean firn temperatures at Eagle and Dome-A are presented in Figure 6. The average 10 m firn temperature over the period 2005-2014 was −58.1°C at Dome-A and −43.1°C at Eagle. Change in the annual mean over the period was small. At Dome-A it was 0.20°C and at Eagle it was 0.24°C. At Eagle, the highest and lowest annual mean temperatures at depths of 3 and 1 m occurred in 2007 and 2009, respectively; the same warm and cold years also occurred in the coastal regions (Figure 5a). By contrast, the highest and lowest annual average temperatures of Dome-A occurred in 2005 and 2012, respectively. The snow or ice temperatures at depths of 3 and 1 m at the Eagle station exhibited almost no change over the decade, whereas Dome-A showed an insignificant temperature decrease. The short-term climate variation at Dome-A differed from both that in the coastal region and the plateau region with small slope.

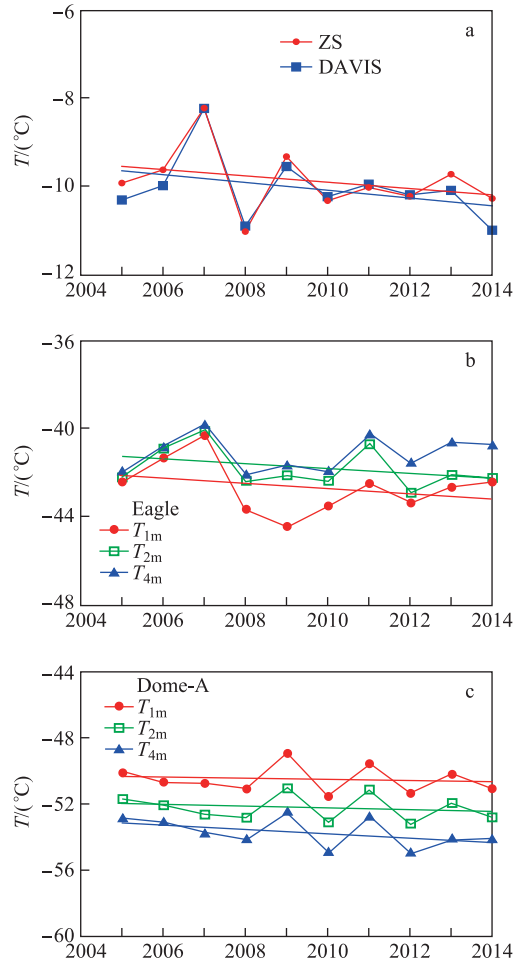

Figure 5 Annual mean temperature (T) from 2005 to 2014 at Zhongshan and Davis Station (**a**), Eagle (**b**) and Dome-A (**c**). Temperature variability is similar at the inland sites to the coast with insignificant trend in annual mean temperature over the decade.

3.3 Surface temperature inversion

On the Australian-built AWS, air temperature is measured at heights of 1, 2, and 4 m above the snow surface (when the station was first deployed). Because of the strong long-wave radiation loss from the snow surface there is almost always a strong surface temperature inversion in the inland ice sheet region (4 m is warmer than 2 m, which is warmer than 1 m). At Dome-A annual average temperature inversion between the 1-m and 4-m instrument levels is more than 3°C (Table 4). This temperature difference is also shown for individual annual mean temperatures at the different measurement levels for both Eagle and Dome-A in Figure 5b and 5c respectively.

The monthly variability of the surface inversion is shown in more detail at Dome-A and Eagle for 2005 in Figure 7. The surface inversion is exceptionally strong at Dome-A, with a very strong seasonal variability, breaking down only in December and January when there is 24-hours of sunlight at the site. In winter, the monthly mean temperature at the 4 m level can be more than 5°C warmer that at the 1 m level. At the windier Eagle site, the inversion is much weaker and has much less seasonal variability

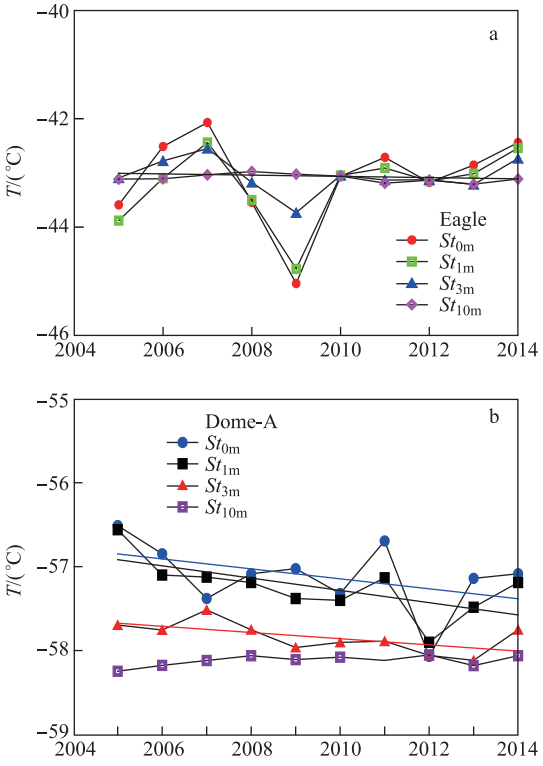

Figure 6 Annual mean firn temperature from 2005 to 2014 at the surface, 1 m, 3 m, and 10 m depth at Eagle (**a**) and Dome-A (**b**)

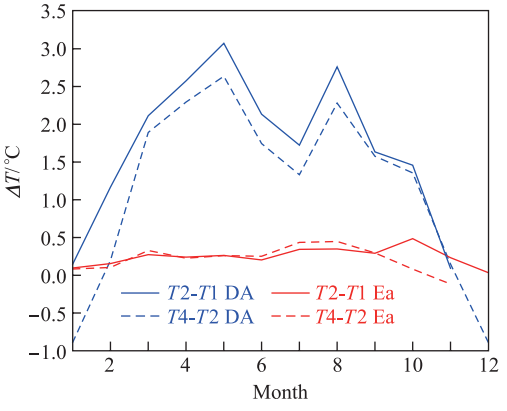

Figure 7 Monthly mean air temperature differences between the 4 m and 2 m levels ($T4-T2$) and between the 2 m and 1 m levels ($T2-T1$) at Dome-A (DA, blue) and Eagle (Ea, red) in 2005.

4 Atmospheric Boundary Layer between ZS and Dome-A

Atmospheric boundary layers of different thickness and elevation result from inhomogeneities in the dynamics and heat budget at the Earth's surface. Understanding the physical process of the interaction between ice or snow and air, and the atmospheric boundary layer structure, is fundamental to improving atmospheric circulation models and numerical

simulations of climate. Except at South Pole and at Dome-C, there are few atmospheric profile observations over the Antarctic inland region[44]. At Dome-C atmospheric temperature, humidity, and boundary layer changes have been observed[45-48]. The Dome-C plateau is characterized by stable weather and an extremely low-temperature inversion layer. More recently, turbulent parameters, annual changes in the radiation balance, and the structure of the boundary layer have also been determined using AWS and atmospheric profile data from the ZS – Dome-A region[24–26, 49-50].

The GPS radiosonde data from Kunlun Station in the summers of 2012 and 2013[24-25] showed that the average rate of decrease of vertical temperature in the troposphere was 5.2°C·km^{-1}, which is lower than the global average lapse rate (~6.5°C·km^{-1}). The mean height of the top of the troposphere was 8.8 km above sea level and the mean temperature there was −51.3°C. Almost all atmospheric water vapour was in the lowest 2 km of the troposphere (Figure 8). Many multi-layer temperature inversion structures existed within the boundary layer, while a strong temperature inversion layer was observed in elevations lower than 500 m (Figure 9). The temperature inversion layer changed with a height lower than 2000 m, and the largest temperature inversion intensity exceeded 3°C·(100 m)$^{-1}$. Two methods, which apply in both stable and unstable conditions, can be used to determine the height of the boundary layer[24]. Either the height of the bottom of the temperature inversion layer is assumed to be the height of the boundary layer (*hb*) or, alternatively, the height where the temperature gradient is largest is taken as the boundary layer height (*h*). Figure 10 presents the relationship between *h* and *hb*. On average, h and hb were 890 and 857.5 m respectively, a difference of only 32.5 m. Therefore, either method can be used to effectively determine the boundary layer top over the Antarctic plateau. The average height of the boundary layer is generally lower in the morning and higher at noon.

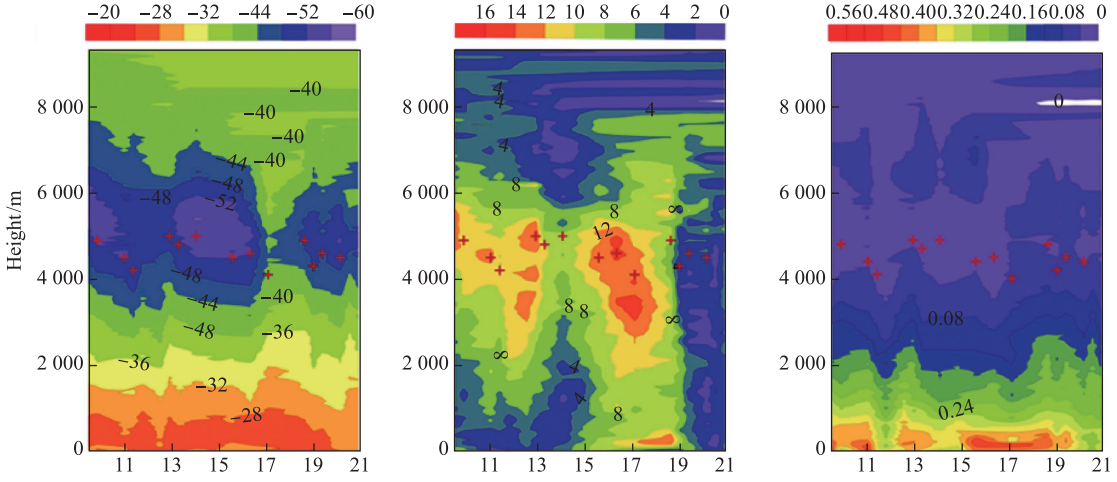

Figure 8 Time-height sections of temperature (°C) (**a**), wind speed (m·s^{-1}) (**b**) and specific humidity (**c**) from GPS radiosonde profiling at Kunlun, 11 to 21 Jan. 2013. Height of Lapse Rate Tropopause (LRT) is shown by + symbols.

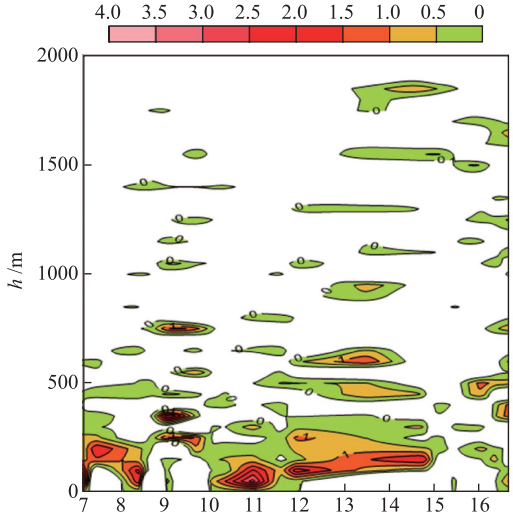

Figure 9 Strength of temperature inversion layers (°C·(100 m)$^{-1}$) in the boundary layer above Kunlun between 7 and 16 Jan. 2013

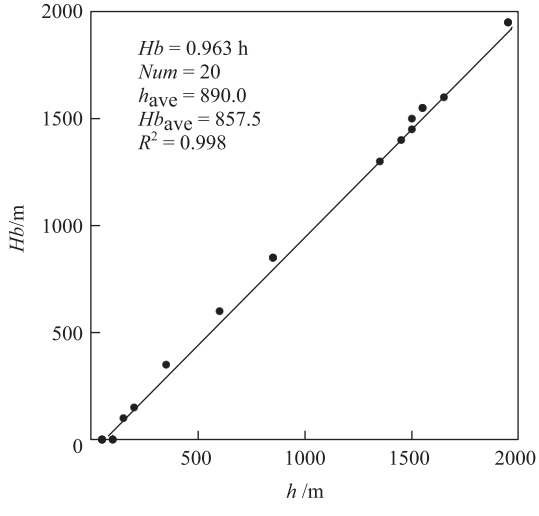

Figure 10 The height of the Planetary Boundary Layer at Kunlun determined from two definitions (see text for details)

5 Turbulent heat exchange and turbulence parameters between ZS and Dome-A

The turbulent heat exchange and turbulence parameters in the surface layer between ZS and Dome-A were determined from AWS data by the aerodynamic (or flux-gradient) method, using 3-years of hourly data at 3 height levels to estimate exchange coefficients, stability correction and fluxes[50,52]. They were also estimated from eddy correlation data obtained from over the ice sheet near ZS in 2007 and in 2008[27-28,50]. Both methods were used to calculate sensible heat flux *SH*, latent heat flux *LE*, surface roughness z_0, atmosphere stability *z/L* (where *L* is the Monin-Obukhov length, the atmospheric height below which turbulence is generated more by buoyancy than by wind shear), and the momentum drag coefficient C_D. Chen et al.[50] studied the seasonal cycle of surface atmospheric parameters over the Antarctic ice sheet in Princess Elizabeth Land, using LGB69 AWS data and compared the results with those from the ZS turbulence measurements[51].

The summer turbulent heat fluxes (*SH* and *LE*) between ZS and Dome-A exhibit a diurnal cycle (Figure 11). Turbulent heat transmitted from the surface snow to the lower atmosphere layer reaches its peak near noon when solar radiation is strongest. The maximum *SH* during the day is approximately 10 W·m^{-2} at ZS, whereas at LGB69 and Dome-A it is around 5 W·m^{-2}, and only about 2 W·m^{-2} at Eagle. The maximum *LE* during the day was 31.1 W·m^{-2} at ZS, 25.5 W·m^{-2} at LGB69, 8.8 W·m^{-2} at Eagle and 2.7 W·m^{-2} at Dome-A. The time at which maximum *LE* transfer occurred is gradually delayed from the coastal region to the inland plateau. This is consistent with the diurnal change of temperature because of the influence of oceanic air mass, which decreases rapidly from the coastal region to the inland plateau. Thus, the air becomes dry and cold. The summer latent heat flux is positive throughout the day at all sites as the snow surface transmits heat to the atmosphere from latent heat of melting or sublimation. The lower atmosphere is gradually stably stratified, with the surface temperature inversion intensifying between afternoon and midnight. *SH* becomes negative after 18:00. The diurnal ranges of *SH+LE* at ZS, LGB69, Eagle, and Dome-A in the summer were 1.4 to 39.2, −0.2 to 30.5, −1.6 to 10.0, and −2.6 to 12.1 W·m^{-2}, respectively. In summer the turbulent heat exchange contributes significantly to the surface energy balance of the coastal region.

The drag coefficient of momentum (C_D) is a critical factor in estimating momentum flux. The mean summer surface friction velocity (*u**), wind speed at 4 m height (*U*), drag coefficient (C_D) and the surface roughness length (z_0) as a function of surface elevation and distance from the coast are shown in Figure 12. Between ZS and Dome-A, the maximum C_D of 1.96×10^{-3} occurred at LGB69 in the steep escarpment and strong katabatic region. It was 1.79×10^{-3} at coastal ZS[51], 1.66×10^{-3} at Eagle, and 1.54×10^{-3} at Dome-A[52]. The strong katabatic wind contributes to momentum transfer. A maximum roughness height, z_0, of 3.05×10^{-4} m was also observed at LGB69. At the coastal ZS it was 2.68×10^{-4} m, and at Eagle and Dome-A it was 2.23×10^{-4} m and 1.45×10^{-4} m, respectively. Roughness height is higher in the strong katabatic wind region, where snow drift frequently occurs and where sastrugi and dunes on the snow surface, together with large snow particles, contribute to a relatively high surface roughness. However, the terrain of the inland plateau is flat with low wind speed. In particular, calm conditions often occur in the Dome-A region, the snow surface is smooth, and the surface roughness is small. The z_0 variations are hence closely related to wind speed [52].

In summer (Dec.−Feb.), the near-surface air is mostly neutrally stratified at all sites. Neutral stability occurs for 85.4%, 91.7%, 87.4%, and 52.5% of the time at ZS, LGB69, Eagle and Dome-A, respectively. Further inland, the periods of both stable and unstable stratification increase. At Dome-A in summer, stable conditions occur for 10.1% of the time while unstable conditions occur for 37.5% of the time. Neutral stratification frequently occurs in the surface atmosphere in the strong katabatic wind region during summer. On the inland plateau, vertical mixing of the atmosphere is relatively weaker because of the low wind speed and persistent surface temperature inversion. Thus, when the surface is heated by solar radiation at noon in summer, surface temperature rapidly increases. However, weak mixing restricts the upward transfer of heat, leading to the observed delay of heating in the higher

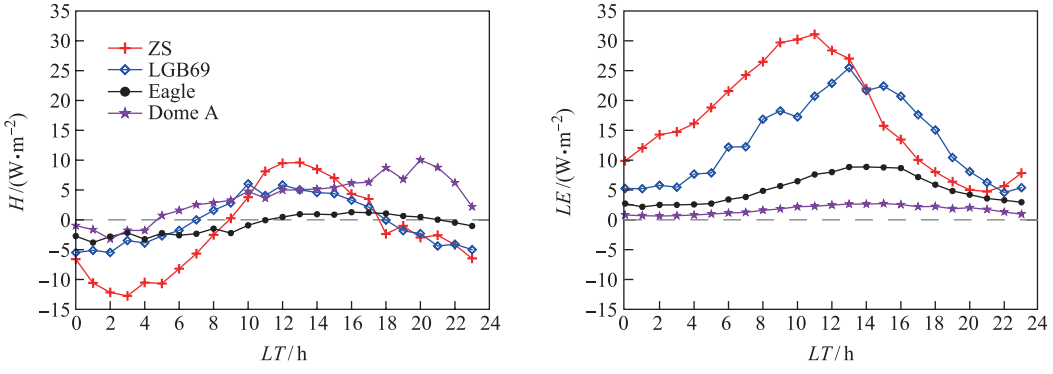

Figure 11 Mean daily cycles of sensible heat flux (*SH*) and latent heat flux (*LE*) for sites between ZS and Dome-A during summer. '*LT*' is local solar time.

atmosphere. On the inland plateau at noon in summer, the surface atmosphere is unstably stratified[23].

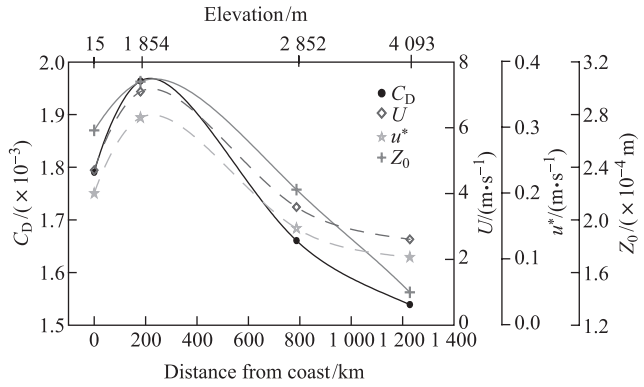

Figure 12 The mean summer (January) surface friction velocity (u_*), wind speed at 4m height (U), drag coefficient (C_D) and the surface roughness length (z_0) as a function of surface elevation and distance from the coast.

6 Radiation Balance

Van den Broeke et al.[14] studied the radiation balance of different Antarctic climatic regions using AWS data from Dronning Maud Land and assessed the role of katabatic wind in the regions. König-Langlo and Augstein[53] examined the seasonal variation of downward long wave radiation over the Antarctic ice sheet and proposed a parameterization for it. Lu et al.[54] analyzed the radiation balance during both polar day and polar night at ZS, which has a short summer and a "coreless" winter, showing that net radiation and annual temperature had a similar pattern of seasonal change. Bian et al.[55] investigated the radiation balance at Great Wall Station and ZS in the Antarctic, detailing seasonal variability of global, absorbed, and reflected solar radiation in the coastal region.

The four AWS between ZS and Dome-A measure only global radiation, and Xiao et al.[43] investigated the relationship between ice sheet elevation and meteorological parameters, including solar radiation. Panda-1 AWS, however, is equipped with four radiation component sensors that obtained continuous data from December 2011 to January 2013 (Figure 13). These radiation sensors are neither heated nor ventilated and hence can experience rime accumulation with unattended operation. To minimize the effect of this, humidity and temperature measurements were used to determine whether apparently abnormal radiation data should be eliminated[49,55]. We use these corrected data to describe all components of the radiation balance at an Antarctic inland site over all seasons.

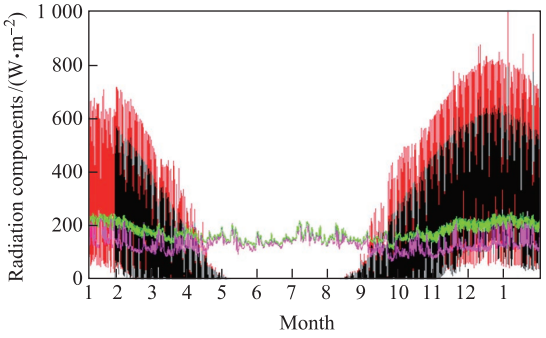

Figure 13 Hourly values of global solar (red), reflected solar (black), upward long wave (green) and downward long wave (pink) radiation at Panda-1 from Jan. 2011 to Jan. 2012.

The maximum global radiation flux at Panda-1 was as high as 990 W·m^{-2} (Figure 13). During the "polar day", the net long wave radiation changes diurnally, with an average flux of 30 W·m^{-2} and a maximum as high as 70 W·m^{-2}. The annual total solar radiation reaching the surface at Panda-1 was 4898 MJ·m^{-2}. The monthly averages of all radiation components at Panda-1 are given in Table 5. Compared with solar radiation, long-wave radiation exhibits lower seasonal changes.

The annual change in surface albedo at Panda-1 is

Table 5 Monthly mean radiation components (W·m^{-2}) at Panda-1 from Feb. 2011 to Jan. 2012

Month	Solar radiation	Reflected radiation	Upward longwave	Downward longwave	Net radiation
1	383.9	316.2	217.0	150.0	0.7
2	257.5	207.7	186.8	123.9	-13.1
3	106.9	81.5	170.1	133.0	-11.7
4	18.2	14.7	160.9	138.5	-18.9
5	0.0	0.0	153.0	138.6	-14.4
6	0.0	0.0	146.5	139.4	-7.1
7	0.0	0.0	171.1	163.0	-8.1
8	4.6	4.0	159.4	145.9	-12.9
9	71.8	51.0	152.1	114.6	-16.7
10	201.9	152.2	164.7	112.6	-2.4
11	360.3	288.6	197.1	122.1	-3.3
12	444.5	363.7	211.4	134.1	3.5

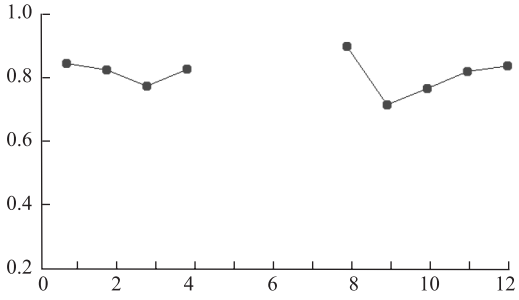

Figure 14 Monthly mean albedo at Panda-1 from Feb. 2011 to Jan. 2012.

shown in Figure 14. This is mainly related to the solar elevation angle. The maximum albedo at the start and end of summer is over 0.8 and fluctuations are high at these times in contrast with midsummer when minimal changes occur. The seasonal variation of albedo at this site suggests frequent snowfall and cloudlessness at the start and end of summer but rare snowfall in the middle of summer.

The net radiation flux over a full year (Table 5) was -8.7 $W \cdot m^{-2}$, which means that the snow surface lost heat. The variation of net radiation over the year is similar to the changes in temperature with a short summer and stable "coreless" winter. The net radiation in winter is negative almost all the time, fluctuating between −10 and −20 $W \cdot m^{-2}$, with only small positive values observed in December and January. The Panda-1 AWS is located on the ice sheet plateau with small slope, and its radiation balance features are expected to be typical of the high latitude inland plateau.

7 Summary

Meteorological observations and investigations undertaken since 2002 over the ice sheet surface between ZS and Dome-A have contributed significantly to our knowledge of climate processes in this region of Antarctica. The AWS and other data have provided new information on short-term climate variability; seasonal and spatial variations of the surface energy balance, radiation and turbulent heat fluxes; the dynamic and thermal parameters of turbulence; and the atmospheric boundary layer structure.

At Dome-A in winter, the surface temperature inversion is persistent and extreme, and the monthly mean temperature at 4 m above the snow surface can be more than 5°C warmer that at the 1 m level. As a result of this, the temperature at 10-m depth in the firn is considerably colder than the annual average temperature at "screen level" (2 m). The coldest 2-m temperature recorded at Dome A between 2005 and 2014 was −82.5°C in July 2005. In summer the height of the thermodynamic boundary layer is about 900 m and the intensity of the temperature inversion in this boundary exceeds 3.0°C·(100 m)$^{-1}$.

Turbulent sensible and latent heat fluxes, and their seasonal variability, along the ice sheet section between ZS and Dome-A have been estimated from the AWS data. The surface air layer transfers heat to the surface mainly by sensible heat to compensate for the long-wave radiation emitted by the snow surface during winter. In the coastal area, latent heat plays an important role in the surface energy balance, whereas its role on the inland plateau is small. Under neutral stratification conditions, the values of surface roughness z_0 and the drag coefficient C_D reach their maxima in the steep escarpment (katabatic) region where the wind speed and surface topographical features are also greatest. They decrease further inland and are at their minima at Dome A.

Air temperature and snow temperature between the coastal Zhongshan and Dome-A on the inland plateau have not changed significantly in the past decade compared with their inter-annual variability.

Acknowledgements This work was supported by the Chinese Polar Environment Comprehensive Investigation and Assessment Program (Grant no. CHINARE 2015-2016), the authors appreciate the assistance of all staff of CHINARE during data collection. Ian Allison's contribution was supported by the Australian Government's Cooperative Research Centres Program through the Antarctic Climate and Ecosystems Cooperative Research Centre.

References

1 Lu L H, Bian L G, Xiao C D, et al. Recent two decades progresses in study on atmospheric sciences of the polar regions. Acta Meteor Sinica, 2004, 62(5): 672–691 (in Chinese)
2 Schwerdtfeger W. The climate of the Antarctic//Orvig S. World survey of climatology. Amsterdam: Elsevier, 1970, 14: 253–355
3 Allison I, Morrissy J V. Automatic weather stations in the Antarctic. Aust Meteor Mag, 1983, 31(2): 71–76
4 Allison I, Wendler G, Radok U. Climatology of the East Antarctic ice sheet (100°E to 140°E) derived from automatic weather stations. J Geophys Res, 1993, 98(D5): 8815–8823
5 Allison I. Surface climate of the interior of the Lambert Glacier Basin, Antarctica, from automatic weather station data. Ann Glaciol, 1998, 27: 515–520
6 Wendler G, Ishikawa N, Kodama Y. The heat balance of the icy slope of Adelie Land, Eastern Antarctica. J Appl Meteor, 1988, 27(1): 52–65
7 King J C, Anderson P S. Heat and water vapour fluxes and scalar roughness lengths over an Antarctic ice shelf. Bound-Layer Meteor, 1994, 69(1–2): 101–121
8 Bintanja R, van den Broeke M R. The surface energy balance of Antarctic snow and blue ice. J Appl Meteor, 1995, 34(4): 902–926
9 Bintanja R. Surface heat budget of Antarctic snow and blue ice: Interpretation of spatial and temporal variability. J Geophys Res, 2000, 105(D19): 24387–24407
10 van As D, van den Broeke M, van de Wal R. Daily cycle of the surface layer and energy balance on the high Antarctic Plateau. Antarct Sci, 2005, 17(1): 121–133
11 King J C, Anderson P S, Smith M C, et al. The surface energy and mass balance at Halley, Antarctica during winter. J Geophys Res, 1996, 101(D14): 19119–19128
12 Bintanja R, Jonsson S, Knap W H. The annual cycle of the surface energy balance of Antarctic blue ice. J Geophys Res, 1997, 102(D2): 1867–1881
13 Reijmer C H, Oerlemans J. Temporal and spatial variability of the surface energy balance in Dronning Maud Land, East Antarctica. J

Geophys Res, 2002, 107(D24): ACL 9-1–ACL 9-12
14 van den Broeke M, Reijmer C, van As D, et al. Daily cycle of the surface energy balance in Antarctica and the influence of clouds. Int J Climatol, 2006, 26(12): 1587–1605
15 van den Broeke M R, Reijmer C, van As D, et al. Seasonal cycles of Antarctic surface energy balance from automatic weather stations. Ann Glaciol, 2005, 41(1): 131–139
16 Turner J, Colwell S R, Marshall G J, et al. Antarctic climate change during the last 50 years. Int J Climatol, 2005, 25(3): 279–294
17 Bian L G, Jia P Q, Lu L H, et al. Surface energy characteristics of Zhongshan Station during 1990, Antarctica. Sci China Ser B, 1992, 22 (11): 1224–1232 (in Chinese)
18 Bian L G, Lu L H, Jia P Q. Experimental observation on the characteristics of the near-surface turbulence over the Antarctic ice sheets during the polar day period. Sci China Ser D: Earth Sci, 1998, 41(3): 262–268
19 Bian L G, Lu L H, Lu C G, et al. A study of radiative features at the Great Wall and Zhongshan stations of Antarctica. Quart J Appl Meteor, 1998, 9(2): 160–168 (in Chinese)
20 Chen Z G, Bian L G, Xiao C D, et al. Seasonal variations of the near surface layer parameters over the Antarctic ice sheet in Princess Elizabeth Land, East Antarctica. Chin J Polar Sci, 2007, 18(2): 122–134
21 Xiao C D, Qin D H, Bian L G, et al. A precise monitoring of snow surface height in the region of Lambert Glacier basin-Amery Ice Shelf, East Antarctica. Sci China Ser D Earth Sci, 2005, 48(1): 100–111
22 Ma Y F, Bian L G, Xiao C D, et al. Correction of snow accumulation impacted on air temperature from Automatic Weather Station on the Antarctic ice sheet. Chin J Polar Res, 2008, 20(4): 299–309 (in Chinese)
23 Ma Y F, Bian L G, Xiao C D, et al. Near surface climate of the traverse route from Zhongshan Station to Dome A, East Antarctica. Antarct Sci, 2010, 22(4): 443–459
24 Fu L, Xian C D, Bian L G, et al. Vertical structure of the atmosphere on east Antarctic plateau. Plateau Meteor, 2015, 34(2): 299–306 (in Chinese)
25 Wang J Z, Bian L G, Xiao C D, et al. Ekman dynamics of the atmospheric boundary layer over the Antarctic Plateau in summer. Chin Sci Bull, 2014, 59(11): 999–1005 (in Chinese)
26 Lin Z, Bian L G, Ma Y F, et al. Turbulent parameters of the near surface layer over the ice sheet near Zhongshan Station, East Antarctica. Chin J Polar Res, 2009, 21(3): 221–233 (in Chinese)
27 Rinke A, Ma Y F, Bian L G, et al. Evaluation of atmospheric boundary layer-surface process relationships in a regional climate model along an East Antarctic traverse. J Geophys Res, 2012, 117(D9): D09121
28 Zhou M Y, Zhang Z H, Zhong S Y, et al. Observations of near-surface wind and temperature structures and their variations with topography and latitude in East Antarctica. J Geophys Res, 2009, 114(D17): D17115
29 Xie A H, Allison I, Xiao C D, et al. Assessment of air temperatures from different meteorological reanalyses for the East Antarctic region between Zhongshan and Dome A. Sci China Earth Sci, 2014, 57(7): 1538–1550
30 Xie A H, Allison I, Xiao C D, et al. Assessment of surface pressure between Zhongshan and Dome A in East Antarctica from different meteorological reanalyses. Arct Antarct Alp Res, 2014, 46(3): 669–681
31 Xie A H, Xiao C D, Ren J W. Correlation between NCEP/NCAR reanalyzed air temperatures and the observed air temperatures from automatic meteorological stations along the route from Zhongshan Station to Dome A, East Antarctica. J Glaciol Geocryol, 2010, 32(5): 898–905 (in Chinese)
32 Savage C R. Automatic weather stations 1980-1981. Antarctic Journal of the United States, 1981, 42(5): 56–62
33 Yasunari T, Kodama S. Intraseasonal variability of katabatic wind over east Antarctica and planetary flow regime in the southern hemisphere. J Geophys Res, 1993, 98(D7): 13063–13070
34 Reijmer C H, van Meijgaard E, van den Broeke M R. Evaluation of temperature and wind over Antarctica in a Regional Atmospheric Climate Model using 1 year of automatic weather station data and upper air observations. J Geophys Res, 2005, 110(D4): D04103
35 Yang Q H, Yin T, Zhang L, et al. Analyses of surface winds along the track from Zhongshan Station to Dome-A, Antarctica. Chin J Polar Res, 2007, 19(4): 295–304 (in Chinese)
36 Xu C. The synoptic characteristics of winter cold and warm days at Zhongshan station. Chin J Polar Res, 2005, 17(2): 115–120 (in Chinese)
37 Xu C, Wang J, Lü F. Statistic and synoptic analysis on blowing snow and snowstorm at Zhongshan station, Antarctica. Chin J Polar Res, 2004, 16(1): 39–45 (in Chinese)
38 Ding Z M, Zhang L, Bian L G, et al. Analysis of katabatic winds on the coast of Prydz Bay. Chin J Polar Res, 2015, 27(4): 351–363 (in Chinese)
39 Bian L G, Ma Y F, Lu C G, et al. Temperature variations at the Great Wall Station (1985–2008) and Zhongshan Station (1989–2008), Antarctic. Chin J Polar Res, 2010, 22(1): 1–9 (in Chinese)
40 Bian L G, Ma Y F, Lu C G, et al. Climate characteristics of precipitation and wind as well pressure and cloud amount at the Great Wall Station (1985–2008) and Zhongshan Station (1989–2008), Antarctic. Chin J Polar Res, 2010, 22(4): 321–333 (in Chinese)
41 Ding M H, Xiao C D, Yang Y D, et al. Re-assessment of recent (2008–2013) surface mass balance over Dome Argus, Antarctica. Polar Res, 2016, 35: 26133
42 Xiao C D, Li Y S, Allison I, et al. Surface characteristics at Dome A, Antarctica: First measurements and a guide to future ice-coring sites. Ann Glaciol, 2008, 48(1): 82–87
43 Chen B L, Zhang R H, Xiao C D, et al. Analyses on the air and snow temperatures near the ground with observations from an AWS at Dome A, the summit of the Antarctic Plateau. Chin Sci Bull, 2010, 55(14): 1430–1436
44 Wang P, Wu X Q. Statistical analysis of temperature and wind speed profiles above the South Pole. J Atmos Environ Opt, 2013, 8(5): 334–343 (in Chinese)
45 Aristidi E, Agabi K, Azoui M, et al. An analysis of temperatures and wind speeds above Dome C, Antarctica. Astron Astrophys, 2005, 430(2): 739–746
46 Tomasi C, Petkov B, Benedetti E, et al. Characterization of the atmospheric temperature and moisture conditions above Dome C (Antarctica) during austral summer and fall months. J Geophys Res, 2006, 111(D20): D20305
47 Mastrantonio G, Malvestuto V, Argentini S, et al. Evidence of a convective boundary layer developing on the Antarctic Plateau during the summer. Meteor Atmos Phys, 1999, 71(1–2): 127–132
48 King J C, Argentini S A, Anderson P S. Contrasts between the summertime surface energy balance and boundary layer structure at Dome C and Halley stations, Antarctica. J Geophys Res, 2006, 111(D2): D02105
49 Fu L, Bian L G, Xiao C D, et al. An observational study of the radiation balance on eastern Antarctic Plateau. Acta Meteor Sinica, 2015, 73(1): 211–219 (in Chinese)
50 Chen Z G, Bian L G, Xiao C D, et al. Characteristics of the seasonal variations of the near surface layer parameters on the Antarctic-

ice sheet in Princess Elizabeth Land, East Antarctica. Acta Oceanol Sinica, 2006, 28(1): 35–41 (in Chinese)

51 Bian L G, Zou H, Zhang D Q, et al. Structure and seasonal changes in atmospheric boundary layer on coast of the East Antarctic continent. Adv Polar Sci, 2013, 24(3): 139–146

52 Ma Y F, Bian L G, Xiao C D, et al. Characteristics of near surface turbulent parameters along the traverse route from Zhongshan station to Dome A, East Antarctica. Chin J Geophys, 2011, 54(8): 1960–1971 (in Chinese)

53 König-Langlo G, Augstein E. Parameterization of the downward long-wave radiation at the Earth's surface in polar regions. Meteor Z, 1994, 3: 343–347

54 Lu L H, Bian L G, Jia P Q. The characteristics of radiation during the Polar day and night at Zhongshan Station, Antarctica. Chin Sci Bull, 1993, 38(6): 475–479

55 Bian L G, Lu L H, Zhang Y P. Some Characteristics of the surface radiation components at Zhongshan station. Antarct Res, 1993, 4(1): 35–41